



Electrodeposition of ZnTe Film with High Current Efficiency at Low Overpotential from a Citric Acid Bath

Takahiro Ishizaki,^z Takeshi Ohtomo, and Akio Fuwa*

Department of Material Science and Engineering, School of Science and Engineering, Waseda University,
Tokyo 169-8555, Japan

The cathodic electrodeposition of ZnTe film was studied using an aqueous citric acid bath (pH 4; temperature 368 K) in which Zn(II) and Te(IV) species were dissolved to form $\text{Zn}(\text{Cit})_2^{4-}$ and HTeO_2^+ ions, respectively. The deposition mechanism was studied based on cyclic voltammetry. The influence of the deposition potential on the morphology, composition, and structure of the deposited film was also investigated. A smooth, dense polycrystalline ZnTe film with nearly stoichiometric composition was deposited at a constant cathode potential, ranging from -0.80 to -0.60 V vs. Ag/AgCl, from a solution containing 20 mmol dm^{-3} Zn(II), $0.16 \text{ mmol dm}^{-3}$ Te(IV), 0.25 mol dm^{-3} H_3Cit , and 0.25 mol dm^{-3} Na_3Cit (Cit = $\text{C}_6\text{H}_5\text{O}_7$). Potentials in this range provided the deposited ZnTe film with high current efficiency (above 98%). During electrodeposition of the nearly stoichiometric crystalline ZnTe, the current density was approximately stationary.

© 2004 The Electrochemical Society. [DOI: 10.1149/1.1643738] All rights reserved.

Manuscript submitted April 22, 2003; revised manuscript received September 22, 2003. Available electronically January 29, 2004.

Zinc telluride (ZnTe) is well known as a II-VI compound semiconductor suitable as window material when employed as a very thin layer in a heterojunction cell or in a n-i-p cell.¹ ZnTe is usually p-type. In addition to fabrication techniques such as metallorganic chemical vapor deposition, molecular beam epitaxy, or vacuum deposition, electrodeposition has also been employed for the fabrication of thin film composed of II-VI compounds. Among these various techniques, electrodeposition can be potentially an interesting cost-effective area processing technique. Electrodeposition from aqueous electrolytes also offers the advantage of being a low-temperature process. Much research has been performed on the electrodeposition of the tellurides, CdTe^{2-11} and $\text{Cd}_x\text{Hg}_{1-x}\text{Te}$,¹²⁻¹⁴ and on the Zn chalcogenides, ZnO ,^{15,16} ZnSe ,¹⁷ ZnHgSe ,^{18,19} and ZnTe .²⁰⁻²⁶ ZnTe has usually been electrodeposited at a relatively negative potential, which indicates that a parallel reaction also proceeds, *i.e.*, hydrogen evolution reduction (HER). HER reduces the current efficiency of the electrochemical process. In order to suppress HER and achieve higher current efficiency, either a higher pH solution has been employed or electrodeposition has been conducted at a potential more positive than would allow HER. However, increasing pH limits the solubility of Te species. Thus, an acidic sulfate solution with a pH of 1-3.5 is often employed for electrodeposition of ZnTe,^{21,25} which is conducted at a more positive potential than the redox potential of the less noble species (in this case, Zn[II]), while employing a diffusion-limiting current for the more noble species (*i.e.*, Te[IV]). Accordingly, an appropriate [Zn(II)]/[Te(IV)] concentration ratio in the acid electrolytic bath, allowing the deposition of stoichiometric ZnTe, is determined by the diffusion-limiting current of the Te reduction, *i.e.*, the concentration of Te^{4+} or HTeO_2^+ ions. Because the solubility of Te species in the acid bath is quite low,²⁷ the deposition rate of ZnTe from the acid bath is also extremely low.

However, it has come to light recently that the solubility of the Te(IV) species in the acid bath could be increased by the use of a new precursor²³ or a complexing agent.²⁸ The former is the use of the existence of possible high supersaturation of dissolved tellurium oxide, which was introduced as a special precursor m-TeO_2 , *i.e.*, metastable TeO_2 . The use of the new precursor made the stoichiometric ZnTe deposition possible from a weak acidic solution (pH 4.5) and allowed higher solubility of Te(IV) species in the electrolytic solution. The latter is the use of citric acid as complexing agent. Although the electrodeposition of CuInSe_2 films from a citric

acid solution has been reported by Pottier *et al.*,²⁹ there are few reports on the electrodeposition of compound semiconductor containing Te from a citric acid solution.

The solubility of TeO_2 as HTeO_2^+ ions at pH 3 is, for example, $10^{-5} \text{ mol dm}^{-3}$, but with citric acid added it improves to about $10^{-2} \text{ mol dm}^{-3}$. Therefore, the deposition rate of ZnTe from a citric acid bath can be expected to increase. Despite the high solubility of Te species in a citric acid bath, little is known about the electrodeposition characteristics of ZnTe prepared from such a bath. In this paper, we report a single electrochemical process for the direct deposition of ZnTe and characterize it according to the effects of (i) the cathode potential (*i.e.*, cathode overpotential), (ii) the Zn and Te species composition of the bath, and (iii) the citrate. ZnTe samples were characterized by X-ray diffraction (XRD), scanning electron microscopy (SEM), energy-dispersive X-ray analysis (EDAX), and inductively coupled plasma atomic emission spectrometry (ICP-AES).

Experimental

Citric acid aqueous electrolytes containing ZnSO_4 , TeO_2 , $\text{C}_6\text{H}_8\text{O}_7 \cdot \text{H}_2\text{O}$ ($\text{H}_3\text{Cit} \cdot \text{H}_2\text{O}$), and $\text{Na}_3\text{C}_6\text{H}_5\text{O}_7 \cdot 2\text{H}_2\text{O}$ ($\text{Na}_3\text{Cit} \cdot 2\text{H}_2\text{O}$) were employed for the ZnTe electrodeposition. All chemicals were of a reagent grade and were used without pretreatment. Deionized water ($7.5 \times 10^6 \Omega \text{ cm}$) was obtained from an Autostill water system (Yamato Co., Ltd., WG25). Table I summarizes the concentrations of Zn and Te and the pH of the citrate electrolytes employed. Electrolytes of various zinc and tellurium concentrations were prepared from ZnSO_4 , TeO_2 , and distilled-deionized water as shown in Table I. Each Zn-Te-citrate bath was obtained by dissolving the appropriate amounts of Zn and Te. The dissolution process was carried out while stirring the mixed solution for several tens of minutes. After complete dissolution, the mixed solutions were extremely stable against the precipitation of Te species. For the pH 4 solutions, there was no visible precipitation of Te(IV) species even when the Te concentration was increased to 1 mmol dm^{-3} (not shown in Table I). It has been reported by Neumann-Spallart and Königstein²⁴ that an optimal pH range for the ZnTe electrodeposition was 4.0-5.5. Thus, the pH of the solutions used for our experiments was *ca.* 4.0, keeping an equal concentration ratio between citric acid and sodium citrate ions (*i.e.*, $[\text{Na}_3\text{Cit}]/[\text{H}_3\text{Cit}] = 1$) and with the temperature maintained by rubber heater at 368 K in all cases. The pH of the electrolytic bath was measured with a conventional glass electrode calibrated using saturated KCl aqueous solution. The pH was measured at a room temperature of 298 K, whereas all electrolytic experiments were carried out at 368 K. Cathodic electrodeposition was performed under potentiostatic conditions using a conventional three-electrode setup comprised of both a potentiostat (Hokuto Denko HA-501)

* Electrochemical Society Active Member.

^z E-mail: isizaki@moegi.waseda.jp

Table I. Electrolytic bath composition and operating conditions employed for deposition of ZnTe.^a

Sample	Concentration (M = mol dm ⁻³)					pH
	ZnSO ₄ (mM)	TeO ₂ (mM)	H ₃ Cit (mM)	Na ₃ Cit (mM)	[Cit] _{total} (mM)	
1	50	0.16	250	250	500	4.0
2	30	0.16	250	250	500	4.0
3	20	0.16	250	250	500	4.0
4	10	0.16	250	250	500	4.0
5	5	0.16	250	250	500	4.0
6	1	0.16	250	250	500	4.05
7	2	0.5	250	250	500	4.05
8	0.5	0.16	250	250	500	4.05

^a Cathode potential ranges were from -0.55 to -0.95 V vs. Ag/AgCl.

connected to a function generator (Hokuto Denko HB-104) and a coulometer (Fuso Seisakujyo HECS-343B). An Ag/AgCl electrode immersed in saturated KCl was used as a reference. Except as otherwise stated, electrode potentials are quoted vs. Ag/AgCl. Cyclic voltammetry (CV) measurements were conducted by scanning the potential of the working electrode at a constant rate of 10 mV s⁻¹. In order to examine the electrode reaction from a Zn-Te-citrate bath, it is necessary to consider the complex formation constant of Zn-citrate and Te-citrate. However, there is no available data for that of Te-citrate. It is well known that Zn and citrate ions form the complex as ZnH₂Cit⁺, ZnHCit, ZnCit⁻, and Zn(Cit)₂²⁻, as shown in the literature.³⁰ The pK of complex formation constant is 1.25, 2.98, 4.98, and 5.90, respectively. In these ion species, Zn(Cit)₂²⁻ is shown the most existing ion species in the electrolytic solution from the complex equilibrium calculation. Thus, the complex formation constant of Zn and citric acid was used as pK = 5.90.³⁰ The dissociation constant of the citric acid was used as pK₁ = 2.87, pK₂ = 4.35, and pK₃ = 5.69,³⁰ where K₁, K₂, and K₃ was thought as follows: K₁[H₃Cit] = [H⁺][H₂Cit⁻], K₂[H₂Cit⁻] = [H⁺][HCit²⁻], and K₃[HCit²⁻] = [H⁺][Cit³⁻]. A gold-plated copper sheet (20 × 40 mm) and a platinum sheet (50 × 50 mm) were employed, respectively, for the working and counter electrodes. The gold plating (thickness ca. 2 μm) was carried out using a gold-plating aqueous solution (Electroplating Engineers of Japan, Ltd., microfab Au310) under galvanostatic conditions of 4 mA cm⁻² at 323 K. Before gold plating, the copper sheets were polished with 6, 1, and 0.3 μm diamond paste, cleaned with distilled water, and degreased. Part of the working electrode surface was covered with Teflon adhesive tape so that a known area (10 × 10 mm) was exposed to the electrolytic solution as the cathode surface. A glass vessel (capacity 250 cm³) with a rubber heater was used as an electrolytic cell. The electrolytic solution was stirred at 400 rpm with a magnetic stirring unit for all runs. In order to avoid any influence from dissolved oxygen, the electrolyte was deaerated by bubbling pure argon gas through it for about 20 min, after which the flux was kept over the electrolytic solution. Film deposition was carried out potentiostatically with the total quantity of electricity being 1.0 C cm⁻². The composition of the deposits was determined quantitatively using EDAX (Horiba EX200) and/or inductively coupled plasma ICP-AES (IRIS-AP). In the latter case, the deposit was dissolved in 1 cm³ of 13 mol dm⁻³ nitric acid and the solution was diluted with distilled water to finally reach 100 cm⁻³. In all cases, the reproducibility of the composition data was checked by duplicate runs under the same experimental conditions. Experimental error for the composition of the obtained deposits was thus determined to be within 3%. The surface morphology of the obtained deposits was observed by SEM (Hitachi S-3000N). XRD (Rigaku RADII-C) was conducted to examine the crystal structure of the deposits. XRD data were obtained using a powder diffractometer with Cu Kα radiation between 20 and 60° at a scanning rate of 2θ

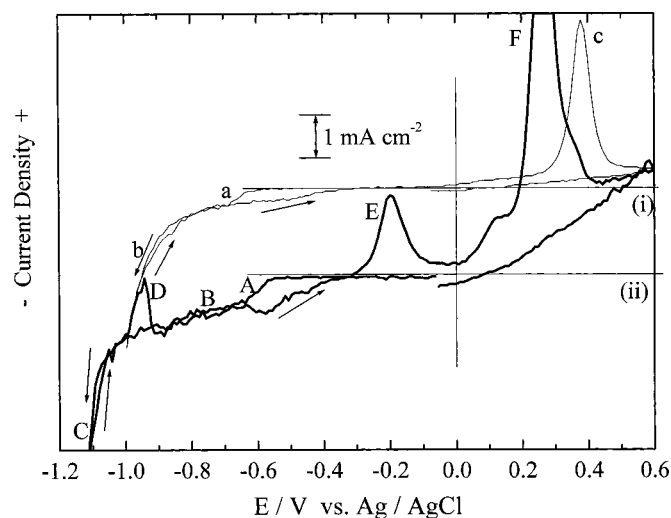
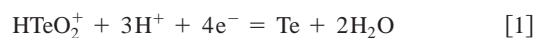


Figure 1. CVs for citric acid solutions ([Cit]_{total} = 0.5 mol dm⁻³, pH = 4.0) containing 0.16 mmol dm⁻³ Te(IV) at 368 K: (i) without Zn(II) and (ii) with 20 mmol dm⁻³ Zn(II). Sweep rate 10 mV s⁻¹.

= 4° (degrees min⁻¹). The XRD peaks were assigned based on JCPDS data. The current efficiency for the ZnTe obtained was calculated as 100(Q_{Zn} + Q_{Te})/Q_{total}, where Q_{Zn} and Q_{Te} indicate the charges for the deposited masses of Zn and Te, respectively, whose depositions are assumed to be two- and four-electron reduction. Q_{total} is the total quantity of charge passed during the electrodeposition.

Results and Discussion

Cyclic voltammetry.—CV was used to study the reactions taking place during film deposition and to find the appropriate deposition potential range for ZnTe. Measurements were carried out at 368 K in an aqueous solution containing 20 mmol dm⁻³ ZnSO₄, 0.16 mmol dm⁻³ TeO₂, 0.25 mol dm⁻³ citric acid, and 0.25 mol dm⁻³ sodium citrate (*i.e.*, the sum of the citrate concentration was 0.5 mol dm⁻³). All voltammograms were first scanned in the cathodic direction, with negative current density indicating a cathodic current. Figure 1 shows two typical CVs obtained with a gold-plated electrode in the electrodeposition bath, where (i) is a tellurium-citrate system between 0.60 and -1.0 V and (ii) is a zinc-tellurium-citrate system between 0.60 and -1.15 V. In (i), when scanning toward more negative potentials, the first cathodic wave, a, appearing at -0.60 V corresponds to the cathodic reduction of HTeO₂⁺ to Te. The charge-transfer reaction proceeds as



The second wave, b, at about -0.85 V could be ascribed to the formation of hydrogen and/or the reduction of the solvent. Beyond this potential range, the further reduction of Te to HTe⁻ proceeds as



At lower pH, the corresponding reduction reaction is



We also observed this reduction reaction on Ti.³¹

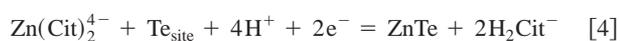
The (i) voltammogram exhibits a small anodic plateau between around 0 and 0.30 V, indicating the beginning of the oxidation of Te by the reverse process of Reaction 1. Based on the Pourbaix diagram,²⁷ the anodic peak, c, at 0.40 V can be ascribed to the oxidation of Te according to the inverse process of Reaction 1.

The large peak separation of waves a and c due to $\text{Te}/\text{HTeO}_2^+$ redox shows that Reaction 1 is irreversible.

The addition of ZnSO_4 in scan (ii) resulted in a sluggish increase of the cathodic current wave, B, and a positive shift in the deposition potential A. This indicates an important change in the reaction mechanism. One possible explanation is that underpotential deposition (UPD) of Zn occurred on the adsorption sites with Te precursors in the same manner as has been discussed for CdTe deposition.³² According to Kröger's analysis,³ ZnTe formation must be preceded by the diffusion-controlled formation of Te on the substrate surface, which then controls the rate of subsequent ZnTe formation. The subsequent UPD of Zn is driven by the negative free energy of the Te and Zn compound formation. Based on this interpretation, by using a simple thermodynamic model of electrochemical reaction and assuming a two-electron transfer reaction for Zn, the overall reaction of ZnTe can be thought of as following two steps

Step 1: Deposition of Te according to Eq. [1].

Step 2: Formation of ZnTe by the following reaction

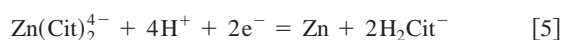


where $\Delta G = -141.6 \text{ kJ mol}^{-1}$.³ The negative free energy ΔG of the formation of ZnTe leads to a positive shift in the potential ΔE for the deposition potential of Zn, as given by

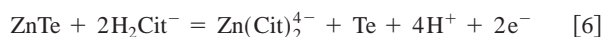
$$\Delta E = -\Delta G/nF = 0.734 \text{ V}$$

Therefore, the total cathodic current is comprised of the deposition reaction of Te and that of Zn due to the formation of ZnTe.

The reduction peak, C, at -1.1 V can be assigned to the reduction of elemental Zn, proceeding as



Several anodic peaks corresponding to the cathodic current are also observed in the voltammogram for (ii). The anodic peak, D, at -0.92 V represents the oxidation of elemental Zn. The cathodic current increases near -0.60 V , crosses the forward scan curve, and remains above it until -0.30 V . This indicates electrocrystallization on a foreign substrate, *i.e.*, a decreased deposition overpotential on an already covered surface. Two subsequent peaks, E (at -0.20 V) and F (at $+0.30 \text{ V}$), can be ascribed to the oxidative decomposition of ZnTe to $\text{Zn}(\text{Cit})_2^{4-}$ ions, expressed as



followed by the oxidation of resulting bulk Te, just referring to inverse reaction, Reaction 1.

The former peak, E, appears only when Zn(II) ions were present in the solution and its peak potential is higher than the redox potential of bulk Zn deposition.

On the basis of these CV studies illustrated in Fig. 1, we concluded that ZnTe can be deposited above the reduction potential of Zn, *i.e.*, -1.10 V and below the potential where Te reduction begins on Au, *i.e.*, -0.60 V .

Effect of cathode potential.—ZnTe films were electrodeposited potentiostatically on Au-coated Cu substrates at different potentials. Following electrodeposition, the samples with the ZnTe films were removed from the electrolytic bath and washed in boiling distilled water to remove traces of the solvent. They were then dried in an electric oven at 353 K .

Figure 2a-c shows SEM photographs of representative deposits obtained at -0.90 , -0.65 , and -0.55 V , respectively, from a solution containing $20 \text{ mmol dm}^{-3} \text{ ZnSO}_4$, $0.16 \text{ mmol dm}^{-3} \text{ TeO}_2$, $0.25 \text{ mol dm}^{-3} \text{ H}_3\text{Cit}$, and $0.25 \text{ mol dm}^{-3} \text{ Na}_3\text{Cit}$ (solution 3, see Table I). XRD of the deposits formed at potentials more negative than -0.60 V , *i.e.*, ranging from -1.0 to -0.60 V , provided a diffraction peak corresponding to the (111) plane of ZnTe³³ with preferential orientation. However, XRD of deposits formed at potentials

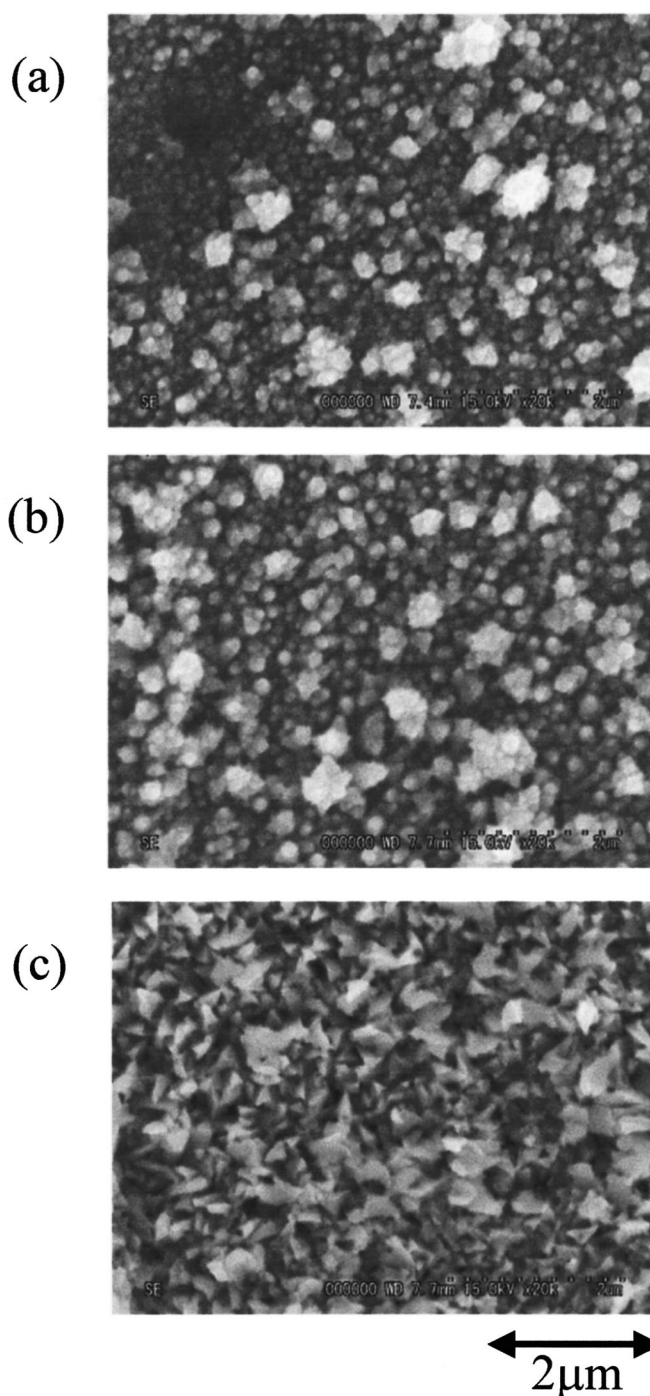


Figure 2. SEM photographs of deposits on polished Au-plated Cu substrate obtained at various potentials from a citric acid bath ($[\text{Cit}]_{\text{total}} = 0.5 \text{ mol dm}^{-3}$, $\text{pH} = 4.0$) containing $0.16 \text{ mmol dm}^{-3} \text{ Te(IV)}$ and $20 \text{ mmol dm}^{-3} \text{ Zn(II)}$ at 368 K : (a) -0.90 , (b) -0.65 , and (c) -0.55 V .

more positive than -0.60 V , *i.e.*, ranging from -0.60 to -0.50 V , displayed a diffraction peak corresponding to the (101) plane of elemental Te³⁴ and no traceable peak corresponding to ZnTe compound. The film electrodeposited at -0.55 V (Fig. 2c) showed dendritic morphology without Zn content. In contrast, the deposits obtained at potentials more negative than -0.60 V displayed only diffraction peaks due to ZnTe and the substrates, *i.e.*, Au and Cu. These deposits appeared to be composed of a reddish-brown film with a dense, granular morphology (Fig. 2b). Their composition was close to stoichiometry, for example, the deposit obtained at -0.65 V

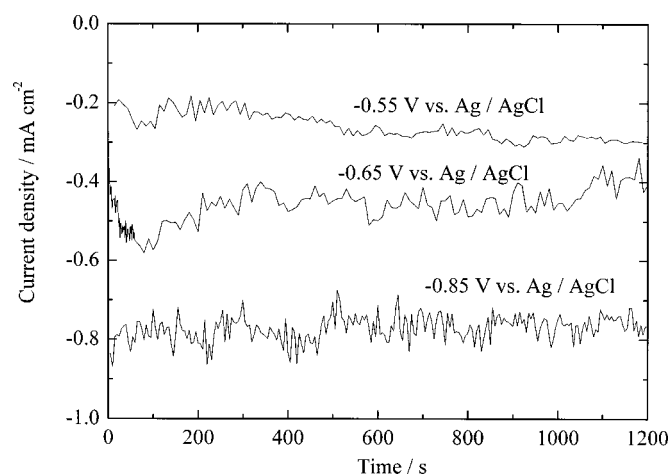


Figure 3. Change in current density during potentiostatic electrodeposition at 368 K from solution 3 where $[\text{Zn(II)}] = 20 \text{ mmol dm}^{-3}$, $[\text{Te(IV)}] = 0.16 \text{ mmol dm}^{-3}$, and $[\text{Cit}]_{\text{total}} = 0.5 \text{ mol dm}^{-3}$.

had a slight Te-rich composition, *i.e.*, 49.2 atom % Zn-50.8 atom % Te. All the deposits obtained at potentials ranging from -0.85 to -0.60 V had a nearly stoichiometric Te-rich composition between 50.7 and 51.2 atom % Te. On the contrary, the deposits obtained at potentials of -0.90 V or more negative had a nearly stoichiometric Zn-rich composition, *i.e.*, 52.5 atom % Zn-47.5 atom % Te at -0.90 V. These deposits appeared to be interference colored and contained sparse spaces partly (Fig. 2a).

Figure 3 shows deposition current *vs.* time transients. The current density during electrodeposition stabilized immediately after the start of the plating and stayed approximately stationary. Figure 4 shows the relationship between the stationary current density, the current efficiency, and the deposition potential. The stationary current density and current efficiency are indicated in the figure by circles and squares, respectively. The stationary current density can be divided into three domains, which are assigned as I, II, and III. In domains I and II, the deposits formed only Te or ZnTe, respectively, as revealed by our XRD peak (see Fig. 5) and composition analysis results. The difference in the constant value of the limiting current density in the different domains may be explained as follows. Assuming that at potentials between -0.50 and -1.0 V the deposition

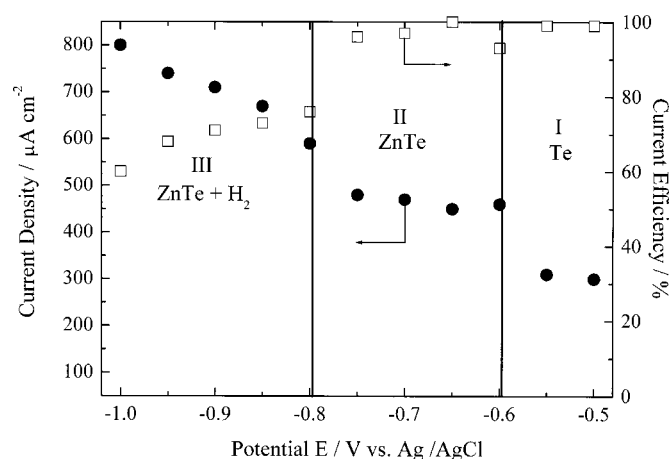


Figure 4. The influence of cathodic potential on stationary current density and current efficiency from solution 3 where $[\text{Zn(II)}] = 20 \text{ mmol dm}^{-3}$, $[\text{Te(IV)}] = 0.16 \text{ mmol dm}^{-3}$, and $[\text{Cit}]_{\text{total}} = 0.5 \text{ mol dm}^{-3}$: (●) constant current densities and (□) current efficiencies.

current density was determined by mass transfer limitation in the stirred solution, the limiting deposition current density of Te(IV) is given as³⁵

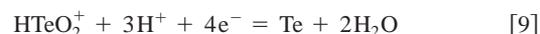
$$J_{\text{Te}} = \frac{4FD_{\text{Te(IV)}}[\text{HTeO}_2^+]}{\delta} \quad [7]$$

Similarly, the current density of ZnTe is given by (assuming that the two-electron transfer reaction for Zn deposition is limited to the covered Te atoms)

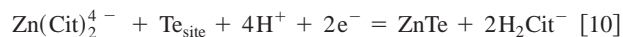
$$J_{\text{ZnTe}} = \frac{6FD_{\text{Te(IV)}}[\text{HTeO}_2^+]}{\delta} \quad [8]$$

where $D_{\text{Te(IV)}}$ is the diffusion coefficient of $[\text{HTeO}_2^+]$ ions (in $\text{cm}^2 \text{ s}^{-1}$), F the Faraday constant (in C mol^{-1}), δ the thickness of the diffusion layer (in cm), and $[\text{HTeO}_2^+]$ the concentration (in mol cm^{-3}). Because the concentration of $[\text{HTeO}_2^+]$ ions in the solution in domains I, II, and III was equal, the limiting current density is proportional to the electrons per molecule reduced, *i.e.*, $J_{\text{ZnTe}}/J_{\text{Te}} = 6/4 = 1.5$. The limiting current density observed at -0.55 V was about $300 \mu\text{A cm}^{-2}$ and that at -0.65 V was about $450 \mu\text{A cm}^{-2}$. The limiting current density proportion obtained from our experimental values, *i.e.*, $J_{\text{ZnTe}}/J_{\text{Te}}$, is about 1.5. This indicates that the deposition of Zn proceeded only on Te atoms. In other words, the large negative free energy of the ZnTe formation acted to drive the deposition of Zn, leading to the formation of ZnTe compound.

This behavior can be explained on the basis of the ZnTe electrodeposition mechanism, considering the competition between two elementary electrochemical steps as suggested by CdTe electrodeposition,³⁶ that is



which is the rate of Te deposition v_1 , and



which is the rate of Zn deposition v_2 .

A single phase of ZnTe forms if the second step, v_2 is faster than the first, v_1 . However, excess Te is left in the deposit if v_2 is somewhat slower than v_1 . In the latter case, two situations can be imagined: one in which diffusion control prevails (*i.e.*, the diffusion is affected by the stirring speed) or another in which the overpotential is too small for the formation of ZnTe (Reaction 4). This second situation occurred when potentials more positive than -0.60 V provided only Te deposits. In these cases, the rate v_1 was faster than v_2 . On the contrary, potentials ranging from -0.60 to -0.80 V provided deposits of ZnTe. Thus, in this potential range, the rate v_2 was faster than v_1 and ZnTe could be fabricated under our experimental conditions. As for domain III, if only ZnTe is electrodeposited, the limiting current density would be *ca.* $450 \mu\text{A cm}^{-2}$. However, the limiting current density we obtained experimentally in domain III ($700\text{--}800 \mu\text{A cm}^{-2}$) was higher than the expected value (*i.e.*, $450\text{--}500 \mu\text{A cm}^{-2}$) and the current efficiency was also lower. It can be thought that this was due to competition from a simultaneous parallel reaction involving HER.

Figure 5 depicts XRD patterns for the deposits obtained at different potentials: (a) -0.90 , (b) -0.75 , (c) -0.65 , and (d) -0.55 V. Peaks due to Au and Cu substrates are indicated in the figure by circles. The films deposited in domains II and III in Fig. 4 are well crystallized with a cubic preferential orientation along the (111) plane, which is characteristic of the spontaneous texture axis of electrodeposited ZnTe. The film deposited in domain II usually appeared reddish-brown, while the film deposited in domain III was interference colored. The interference colors exhibited by the Zn-rich ZnTe were due to the lower thickness of the film, as indicated by its weak XRD intensity. The narrow peak width of the film deposited in domain II (*i.e.*, at the potential range from -0.80 to

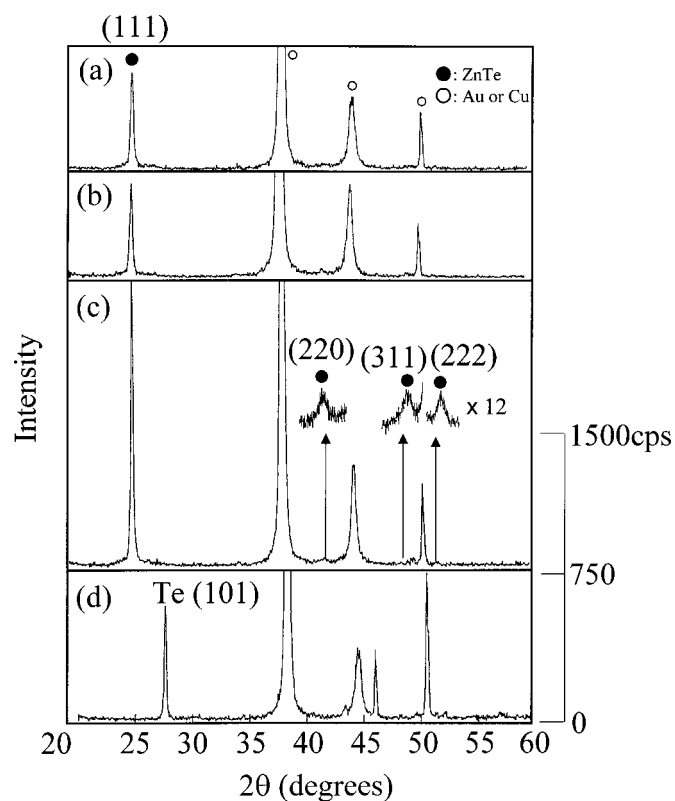


Figure 5. XRD patterns of deposits obtained at various potentials from citric acid electrolytes ($[\text{Cit}]_{\text{total}} = 0.5 \text{ mol dm}^{-3}$, $\text{pH} = 4.0$) containing $0.16 \text{ mmol dm}^{-3}$ Te(IV) and 20 mmol dm^{-3} Zn(II) at 368 K: (a) -0.90 , (b) -0.75 , (c) -0.65 , and (d) -0.55 V. Film thicknesses $0.4\text{--}0.7 \mu\text{m}$.

-0.60 V) indicates high crystallization with large grain size. In contrast, the film deposited in domain I yielded a diffraction corresponding to the (101) plane of crystalline elemental Te.

Thus, nearly stoichiometric ZnTe films with high crystallization were obtained at low overpotential, namely, -0.65 V. Subsequent experiments were therefore carried out at -0.65 V.

Effect of the Zn(II) and Te(IV) concentration ratio.—The $[\text{Zn(II)}]/[\text{Te(IV)}]$ concentration ratio is an important factor for the electrodeposition of highly crystallized ZnTe film and for the electrochemical behavior of the deposited ZnTe. The influence of the $[\text{Zn(II)}]/[\text{Te(IV)}]$ concentration ratio on the films obtained was studied using solutions with various $[\text{Zn(II)}]/[\text{Te(IV)}]$ ratios, *i.e.*, samples 1–8 (see Table I), while maintaining the cathode potential at -0.65 V for all runs.

Table II summarizes the $[\text{Zn(II)}]/[\text{Te(IV)}]$ concentration ratio, the

Table II. Characterization of films electrodeposited from citric acid ZnTe electroplating baths.^a

Sample	Composition (atom %)		$[\text{Zn(II)}]/[\text{Te(IV)}]$ concentration ratio	Color
	Zn	Te		
1	51.0	49.0	312.5	Interference
2	49.7	50.3	187.5	Reddish-brown
3	48.9	51.1	125	Reddish-brown
4	49.1	50.9	62.5	Reddish-brown
5	49.6	50.4	31.25	Reddish-brown
6	50.1	49.9	6.25	Reddish-brown
7	39.9	60.1	4	Blackish-gray
8	4.6	95.4	3.125	Blackish-gray

^a Cathode potential was -0.65 V vs. Ag/AgCl.

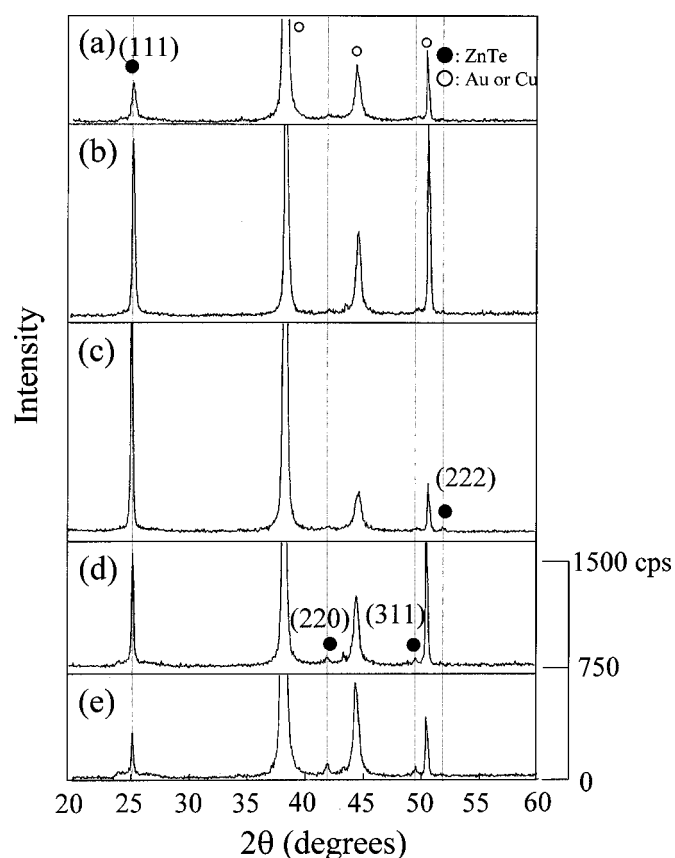


Figure 6. XRD patterns of deposits obtained at 368 K and -0.65 V from citric acid electrolytes ($[\text{Cit}]_{\text{total}} = 0.5 \text{ mol dm}^{-3}$, $\text{pH} = 4.0$) under various Zn(II) concentrations as summarized in Table II: (a) 50, (b) 30, (c) 10, (d) 5, and (e) 1 mmol dm^{-3} .

color, and the composition of the films deposited at -0.65 V. All the films obtained for samples 2–8 had a thickness of about $1 \mu\text{m}$ and consequently showed the color representing the feature as bulk. The films obtained from samples 7 and 8 appeared to be blackish-gray with a dull gloss, indicating a metallic color. According to EDAX analysis, they had a Te-rich composition, *i.e.*, 39.9 atom % Zn–60.1 atom % Te for sample 7 and 4.6 atom % Zn–95.4 atom % Te for sample 8. The film obtained from sample 1 was interference colored and the intensity of its XRD peak corresponding to the (111) plane of ZnTe was broad and weak (see Fig. 6a). The sample 1 film was thinner than those of samples 2–6, indicating that its current efficiency was relatively low (87%); the current efficiencies of samples 2–6 were above 98%. The sample 1 film had a Zn-rich composition, *i.e.*, 51 atom % Zn–49 atom % Te. In contrast, the films obtained from samples 2–6 had near stoichiometric composition and characteristic bulk color (reddish-brown). Figure 6 displays representative XRD patterns for films deposited at different $[\text{Zn(II)}]/[\text{Te(IV)}]$ concentration ratios. The films deposited from samples 2, 4, 5, and 6 (Fig. 6b–e, respectively) exhibit diffraction corresponding to the (111) plane of high-crystalline ZnTe, although the film obtained from sample 1 (Fig. 6a) has broader peak width, indicating low crystallization. It was reported that there was an optimal Zn concentration window for the electrodeposition of the stoichiometric ZnTe film from a weak acidic solution.²³ An optimal Zn concentration window we used was much the same as the report by Königstein *et al.* for obtaining the stoichiometric ZnTe film. As the $[\text{Zn(II)}]/[\text{Te(IV)}]$ concentration ratio in the bath reduced, preferential orientation along the cubic (111) gradually decreased.

Figure 7 shows the variation of the constant current density vs. Zn(II) and Te(IV) concentration. Note that the deposition current is proportional not to the Zn(II) concentration but to the Te(IV) con-

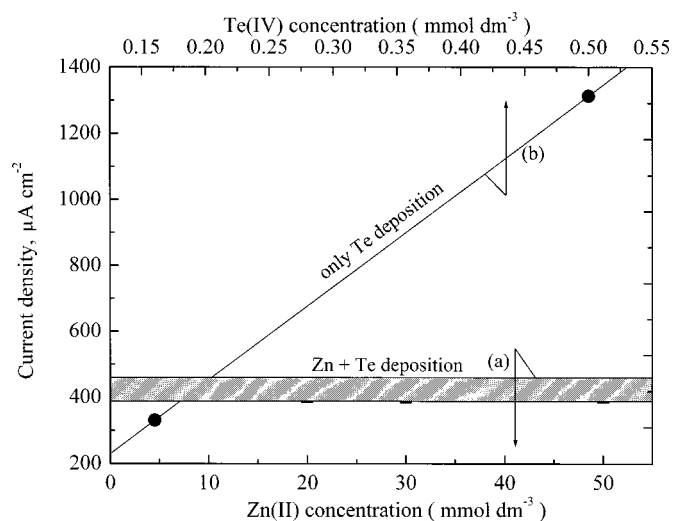


Figure 7. Dependence of the stationary current density at -0.65 V on the concentrations of (●) TeO_2 and (■) ZnSO_4 : (a) the current density at different Te concentrations, with 20 mmol dm^{-3} ZnSO_4 and 0.5 M citrate, and (b) the current density at different Zn concentrations, with $0.16 \text{ mmol dm}^{-3}$ TeO_2 and 0.5 M citrate.

centration. It tended to be constant (*ca.* $420 \mu\text{A cm}^{-2}$) for the deposition of a nearly stoichiometric ZnTe with high crystallization, even when the Zn(II) concentration in the bath increased. This indicates that the plating rate of ZnTe was insensitive to the Zn(II) concentration. This result is in agreement with that reported by Königstein and Neumann-Spallart.²³ This behavior indicates that the growth, *i.e.*, ZnTe formation, depends greatly on diffusion control due to Te deposition. As mentioned previously, when the rate v_2 is faster than v_1 , UPD of Zn onto Te atoms is possible due to the strong interaction between Zn and Te. Kinetic effects may also be involved through the variation of cathode potential and Zn(II) concentration. Thus, a wide range of $[\text{Zn(II)}]/[\text{Te(IV)}]$ concentration ratios, where $[\text{Zn(II)}]/[\text{Te(IV)}] > 6$, allows the formation of ZnTe, and the Zn content in the deposit is almost constant even when the Zn concentration in the bath is increased (see Table II).

When the $[\text{Zn(II)}]/[\text{Te(IV)}]$ concentration ratio is greater than 6, the rate v_2 of the Zn deposition is faster than the rate v_1 of the Te deposition, leading to the formation of ZnTe.

Effect of citrate.—In order to examine the effect of citrate on the properties of the ZnTe deposit, including its composition and crystallinity, solutions containing different citrate concentrations were employed for ZnTe electrodeposition.

Figure 8 depicts two XRD patterns from solutions containing 20 mmol dm^{-3} ZnSO_4 and $0.16 \text{ mmol dm}^{-3}$ TeO_2 at pH 4. The solution for (a) in Fig. 8 contained 0.5 mol dm^{-3} citrate and deposition was onto Au/Cu substrate (keeping $[\text{H}_3\text{Cit}]/[\text{Na}_3\text{Cit}] = 1$). The solution for (b) did not include citrate and deposition was onto Au/Cu substrate. The deposit from a solution containing citrate had diffractions corresponding to the (111) plane of ZnTe and to the substrate used, *i.e.*, Au and Cu, while the deposit from a solution without citrate had a rather broad diffraction instead of the ZnTe(111) peak, indicating that the film was amorphous. When the citrate was present in the bath, there were two conspicuous differences in the XRD patterns: (i) the crystallinity of the ZnTe deposit was higher and (ii) the ZnTe peak was narrower. This indicates that citrate greatly promoted the crystallization of ZnTe and increased crystallite size. Table III shows the composition of Zn and Te in deposits obtained at different citrate concentrations. According to the comparison of the composition of the deposits from a solution with and without citrate, it is clear that the deposition of Zn is depressed. As the citrate concentration in the bath increased, the Zn content in the

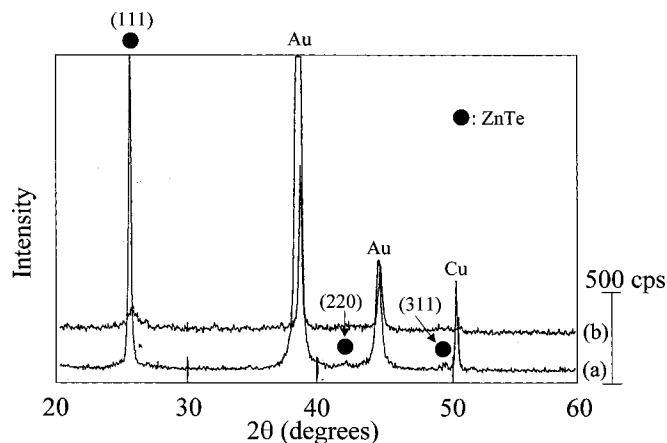


Figure 8. XRD patterns of deposits obtained from citric acidic electrolytes containing $0.16 \text{ mmol dm}^{-3}$ Te(IV) and 20 mmol dm^{-3} Zn(II) . The total quantity of electricity was 1.0 C cm^{-2} and the thickness of films was *ca.* $0.6 \mu\text{m}$: (a) with 0.5 M citrate on Au/Cu substrate and (b) without citrate on Cu substrate at 368 K and -0.80 V .

deposit gradually increased, while the Te content gradually decreased. This indicates that citrate forms a certain complex with Te(IV) species and favors the formation of Te-citrate complex rather than that of Zn-citrate complex. In addition, although ZnTe deposition has frequently been carried out at potentials more negative than -0.80 V , our bath containing citrate allowed the formation of ZnTe at higher potentials, *i.e.*, at a lower overpotential. From these results we concluded that including citrate in the bath depresses the deposition of Te and promotes high ZnTe crystallinity.

Conclusions

In this work, the cathodic electrodeposition of ZnTe in a citric acid bath was carried out at higher potentials, *i.e.*, lower overpotential, than the reduction of Zn(Cit)_2^{4-} to Zn. Films deposited at potentials ranging from -0.60 to -0.80 V were composed of ZnTe compound with quite stoichiometric composition and high crystallization. Their surface morphology was dense and granular. Deposits obtained at potentials more positive than -0.60 V resulted in the formation of blackish-gray colored, crystalline Te. The plating rate of ZnTe was insensitive to the Zn(II) concentration and was controlled by the diffusion of Te species. The formation of ZnTe was accounted for by its electrodeposition mechanism. The deposition of Zn proceeded only on Te-covered substrate and the large negative free energy of the compound formation led to the formation of ZnTe. Including citrate in the bath depressed the deposition of Te and provided high ZnTe crystallinity. When electrolyzed at -0.65 V and 368 K , solutions where $[\text{Zn(II)}] = 1\text{--}50 \text{ mmol dm}^{-3}$, $[\text{Te(IV)}] = 0.16 \text{ mmol dm}^{-3}$, $[\text{Cit}]_{\text{total}} = 0.5 \text{ mol dm}^{-3}$, and pH 4.0 were found to be suitable for the electrodeposition of reddish-brown colored, crystalline ZnTe.

Table III. The effect of citrate on the composition of films electrodeposited from a citric acid ZnTe electroplating bath.^a

Citrate concentration (M = mol dm ⁻³)	Composition (atom %)	
	Zn	Te
0 M	58.4	41.6
0.05 M	45.5	54.5
0.10 M	46.0	54.0
0.50 M	47.8	52.2
1.0 M	52.2	47.8

^a Bath conditions: 20 mM ZnSO_4 , 0.16 mM TeO_2 , 368 K . Cathode potential was $-0.65 \text{ V vs. Ag/AgCl}$.

Acknowledgments

This work is supported by Research Fellowships of the Japan Society for the Promotion of Science for Young Scientists (JSPS).

Waseda University assisted in meeting the publication costs of this article.

References

1. P. V. Meyers, *Sol. Cells*, **23**, 59 (1988).
2. M. P. R. Panicker, M. Knaster, and F. A. Kroger, *J. Electrochem. Soc.*, **125**, 566 (1978).
3. F. A. Kroger, *J. Electrochem. Soc.*, **125**, 2028 (1978).
4. R. N. Bhattacharya, K. Rajeshwar, and R. N. Noufi, *J. Electrochem. Soc.*, **132**, 732 (1985).
5. A. C. Rastogi and K. S. Balakrishnan, *J. Electrochem. Soc.*, **136**, 1502 (1989).
6. S. K. Das and G. C. Morris, *Sol. Energy Mater. Sol. Cells*, **28**, 305 (1993).
7. S. K. Das, *Sol. Energy Mater. Sol. Cells*, **29**, 277 (1993).
8. Y. Guo and X. Deng, *Sol. Energy Mater. Sol. Cells*, **29**, 115 (1993).
9. I. Villegas and J. L. Stickney, *J. Electrochem. Soc.*, **138**, 1310 (1991).
10. K. Murase, H. Uchida, T. Hirato, and Y. Awakura, *J. Electrochem. Soc.*, **146**, 531 (1999).
11. T. Hirato, J. Nakatani, and Y. Awakura, *J. Surf. Finish. Soc. Jpn.*, **48**, 190 (1997).
12. B. M. Basol, E. S.-F. Tseng, and D. S.-H. Lo, Eur. Pat. EP 152197 A2; BE, DE, FR, GB, IT, NL, EP 85-300435; PRAI US 84-576559.
13. M. Neumann-Spallart, G. Tamizhmani, and C. Levy-Clement, *J. Electrochem. Soc.*, **137**, 3434 (1990).
14. M. Neumann-Spallart, G. Tamizhmani, A. Boutry-Forveille, and C. Levy-Clement, *Thin Solid Films*, **169**, 315 (1989).
15. S. Peulon and D. Lincot, *Adv. Mater. (Weinheim, Ger.)*, **8**, 166 (1996).
16. S. Peulon and D. Lincot, *J. Electrochem. Soc.*, **145**, 864 (1998).
17. G. Riveros, H. Gómez, R. Henríquez, R. Schreiber, R. E. Marotti, and E. A. Dalchiele, *Sol. Energy Mater. Sol. Cells*, **70**, 255 (2001).
18. C. Natarajan, M. Sharon, C. Levy-Clement, and M. Neumann-Spallart, *Thin Solid Films*, **237**, 118 (1994).
19. C. Natarajan, M. Sharon, C. Levy-Clement, and M. Neumann-Spallart, *Thin Solid Films*, **257**, 46 (1995).
20. K. K. Mishra and K. Rajeshwar, *J. Electroanal. Chem. Interfacial Electrochem.*, **273**, 169 (1989).
21. B. M. Basol and V. K. Kapur, *Thin Solid Films*, **165**, 237 (1988).
22. A. J. Pason, *Inorg. Chem.*, **3**, 941 (1964).
23. C. Königstein and M. Neumann-Spallart, *J. Electrochem. Soc.*, **145**, 337 (1998).
24. M. Neumann-Spallart and C. Königstein, *Thin Solid Films*, **265**, 33 (1995).
25. B. Bozzini, M. A. Baker, P. L. Cavallotti, E. Cerri, and C. Lenardi, *Thin Solid Films*, **361-362**, 388 (2000).
26. A. B. Kashyout, A. S. Arico, P. L. Antonucci, F. A. Mohamed, and V. Antonucci, *Mater. Chem. Phys.*, **51**, 130 (1997).
27. M. Pourbaix, *Atlas of Electrochemical Equilibria in Aqueous Solutions*, p. 560, Pergamon Press, Oxford (1966).
28. T. Oda, K. Murase, T. Hirato, and Y. Awakura, in *Proceedings of J. Surf. Finish. Soc. Jpn.*, 104th Symposium, p. 146 (2001).
29. D. Pottier and G. Maurin, *J. Appl. Electrochem.*, **19**, 361 (1989).
30. R. M. Smith and A. E. Martell, *Critical Stability Constants*, Vol. 3, p. 161, Plenum Press, New York (1976).
31. T. Ishizaki, D. Yata, and A. Fuwa, *Mater. Trans.*, **44**, 1583 (2003).
32. A. Sarabyreintjes, L. M. Peter, M. E. Özsan, S. Dennison, and S. Webster, *J. Electrochem. Soc.*, **140**, 2880 (1993).
33. JCPDS File, Card No. 15-0746 (unindexed peaks), JCPDS, Swarthmore, PA.
34. JCPDS File, Card No. 36-1452 (unindexed peaks), JCPDS, Swarthmore, PA.
35. A. J. Bard and L. R. Faulkner, *Electrochemical Methods*, p. 32, John Wiley and Sons, Inc., New York (1980).
36. C. Lepiller, P. Cowache, J. F. Guillemoles, N. Gibson, E. Özsan, and D. Lincot, *Thin Solid Films*, **361**, 118 (2000).